Entanglements of Electrons and Cavity Photons in the Strong-Coupling Regime

Ofer Kfir*
University of Göttingen, IV. Physical Institute, Göttingen 37077, Germany

(Received 3 May 2019; published 6 September 2019)

This Letter sets a road map towards an experimental realization of strong coupling between free electrons and photons and analytically explores entanglement phenomena that emerge in this regime. The proposed model unifies the strong-coupling predictions with known electron-photon interactions. Additionally, this Letter predicts a non-Columbic entanglement between freely propagating electrons. Since strong coupling can map entanglements between photon pairs onto photon-electron pairs, it may harness electron beams for quantum communication, thus far exclusive to photons.

DOI: 10.1103/PhysRevLett.123.103602

Entanglement between the states of propagating quantum entities and its violation of local realism [1–3] acquires significant technological importance for quantum technologies, such as quantum computation and quantum key distribution [4]. Polarization of photon pairs, expressed as Bell states, allow for the transport of quantum entanglement over ever-growing distances, under the sea [5] and in outer space [6]. The rich set of properties of matter-wave beams may offer new opportunities for quantum communication and computation. For example, fundamental particles such as electrons are decoupled from free-space radiation, lack an internal structure to decohere into, and their short wavelength may be used to mitigate beam divergence over long distances. Currently, however, the quantum control of electron beams is at its infancy.

Two important phenomena address the energy exchange of light and electron beams: photoinduced near-field electron microscopy (PINEM) and electron-energy loss spectroscopy (EELS). In PINEM [7], a strong (and hence classical) laser field accelerates or decelerates electrons in a beam. This concept allows for optical control over the electron quantum wave function [8–11], culminating in the prediction [8] and demonstration [12–14] of attosecond-scale electron pulses. Similar effects, such as electron-energy gain spectroscopy [15,16], and effects of the light's ponderomotive energy, such as the Kapitza-Dirac effect [17] and electron-phase retarders [18], are also well described by classical laser fields. In the abovementioned effects, adding or removing a photon from the laser field makes no difference, since the electron-photon coupling is extremely weak.

In EELS, the coupling can be increased by using metallic nanostructures. The large polarizability and plasmonic resonances [19] allow for detectable signals, while the nanometric features compensate for the momentum mismatch (see detailed reviews by García de Abajo [20] and Talebi [21] and references within). Such systems were investigated using rings [22], spheres [20], cubes [23,24], and rods [25,26] geometry, as well as for stacked particles [27], ordered or disordered structures [28–30], and also symmetric [31,32] and symmetry-broken systems exhibiting non-Hermitian phenomena [33]. However, rapid decoherence eliminates entanglement features [34] between the electrons and any excited plasmons, stemming from radiative damping [35], intrinsic dissipation [36] absorption, and sensitivity to defects. Alternatively, transparent dielectrics have no theoretical bound for the excitation probability [28]. Optical excitations in such dielectrics can be readily injected, collected, or manipulated, but unfortunately, their coupling to electron beams is weak.

This Letter proposes that the phase matching of swift electrons to photons confined in a waveguide-based dielectric cavity can increase the interaction towards the strong-coupling regime and theoretically investigates emergent entanglement phenomena. The phase-matching bandwidth can isolate even a single cavity mode, allowing for a single channel of energy exchange between matter and radiation. An analytical entanglement model is developed for the electron-cavity interaction, which applies for any coupling regime, weak or strong. To exemplify novel phenomena arising in the strong-coupling regime, this Letter focuses on two scenarios: First, the entanglement between cavity photons and a traversing electron is investigated, and compared to PINEM and EELS in the limit of weak coupling. Through this comparison, I find that, for PINEM driven with a coherent state $|\alpha\rangle$, the Rabi parameter is given by $g = g_{\mathrm{Qu}}\alpha$, where g_{Qu} is the coupling strength. As a second example, the cavity capability to mediate non-Coulombic entanglement between two distant electrons within a beam is explored. Finally, the strength and spectral properties of the coupling are evaluated *quantitatively*, for the case of a racetrack whispering-gallery mode cavity based on a single-mode waveguide.

The proposed approach combines two essential concepts: (i) modal confinement allows for a *meaningful electric field per photon*, and (ii) energy exchanges

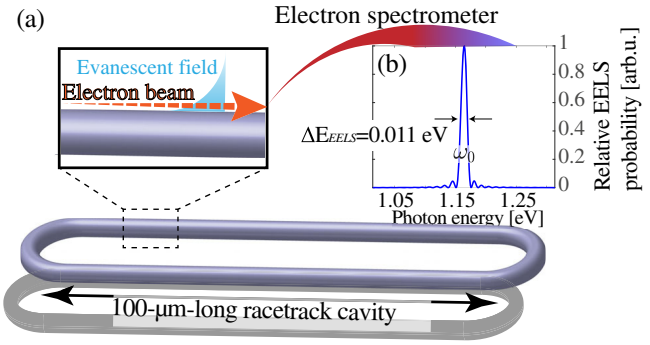

FIG. 1. Proposed experiment for a narrow bandwidth strong coupling. (a) Evanescent optical field couples a cavity mode to an adjacent electron. (b) Phase matching between the electron and the cavity photon limits the coupling to a narrow spectral band. For example, a 100 μm propagation near a Si_3N_4 cavity limits the coupling bandwidth (expressed as EELS bandwidth) to 11 meV around $\hbar\omega_0 = 1.166$ eV ($\lambda = 1064$ nm).

between a light field and a traversing electron is increased by *phase matching* them over an extended length. Thus, the effect of even a single photon can build up coherently along the propagation and approach strong coupling. Those can be realized by using a whispering-gallery mode (WGM) cavity with a racetrack geometry (see Fig. 1). An electron beam passing parallel to a straight section of the cavity, which is a single-mode waveguide, excites the mode via its evanescent tail in the vacuum. The conservation of both energy and momentum (i.e., phase matching) is fulfilled only for a specific photon energy, for which the electron travels at the mode's phase velocity. The interaction spectral bandwidth can be very narrow due to dispersion in the waveguide. In the example of Fig. 1(b), a silicon-nitride (Si_3N_4) cavity is optimized to couple electron beams accelerated to 200 keV with photons having vacuum wavelength near 1.064 μm ($\hbar\omega_0 = 1.166$ eV). The coupling bandwidth narrows down to only 0.011 eV after a propagation of 100 μm. More details are discussed later on.

The analytical model relies on the narrow spectral response of the proposed system. Only photons having angular frequency ω_0 are phase matched with the relativistic electron beam. The narrow bandwidth suppresses finite electron wave packet [37,38] effects. The quantum state of these two systems can be described as energy-ladder systems with $\hbar\omega_0$ spacing between the levels: The photon Fock states in the cavity are represented by $|n\rangle$, a semi-infinite ladder with $n \geq 0$. The electron states $|E_k\rangle$, with $E_k = E_0 + k\hbar\omega_0$, represent gain ($k > 0$) and loss ($k < 0$) with respect to the "zero-loss energy" E_0. $\hbar$ is the reduced Planck's constant. Thus, a general state of such electron-photon system can be written as

$$|\psi\rangle = \sum_{n=0}^{\infty}\sum_{k=-\infty}^{\infty} c_{n,k}|E_k, n\rangle. \tag{1}$$

The relation between the state of the system before and after the interaction can be described by the scattering matrix $\hat{S}$ as $|\psi_{\text{final}}\rangle = \hat{S}|\psi_{\text{initial}}\rangle$. Neglecting electron dispersion effects allows one to write $\hat{S}$ as an operator that exchanges energy between the electrons and the photons,

$$\hat{S} = D(\hat{b}g_{\text{Qu}}) = e^{g_{\text{Qu}}\hat{b}\hat{a}^\dagger - g_{\text{Qu}}^*\hat{b}^\dagger\hat{a}}. \tag{2}$$

$\hat{a}$ and $\hat{a}^\dagger$ are the noncommuting photon-ladder operators, and $\hat{b}$ and $\hat{b}^\dagger$ are the commuting electron-energy-ladder operators. The commutation $[\hat{b}, \hat{b}^\dagger] = 0$ results in an algebra similar to scalars, so $\hat{S}$ behaves as the displacement operator $D(g_{\text{Qu}})$ [39]. A comprehensive treatment of $\hat{b}$, $\hat{b}^\dagger$ and electron dispersion effects can be found in Secs. S.4 and S.1 of the Supplemental Material [40], respectively. Although $g_{\text{Qu}} \geq 1$ is the obvious definition for the strong-coupling regime, some strong-coupling phenomena, e.g., energy transfers of multiple quanta, emerge already for moderate couplings.

The interaction of a relativistic electron with an empty cavity is an important and instructive case to consider [see Fig. 2(a)]. The initial state of the electron-photon system is a pure state, with the electron at the zero-loss energy and no photons

$$|\psi_i\rangle = |E_0, 0\rangle. \tag{3}$$

Since the interaction is a displacement operator, the state after the interaction $|\psi_f\rangle$ is a coherent state [43], as for plasmons [44]. The conservation of energy entangles each optical Fock state to an equal electron-energy loss $E_k = E_{-n}$, therefore

$$|\psi_f\rangle = \sum_{n\geq 0}^{\infty} e^{-|g_{\text{Qu}}|^2/2}\frac{g_{\text{Qu}}^n}{\sqrt{n!}}|E_{-n}, n\rangle. \tag{4}$$

One can consider Eq. (4) as the multilevel electron-photon equivalent of a Bell pair, $|\psi_f\rangle = (c_0|E_0, 0\rangle + c_1|E_{-1}, 1\rangle + \cdots)$. Thus, coincidence measurements should expose correlations between the measured electron-energy loss and photon detection. The equivalence to EELS experiments is retrieved for weak couplings, where only one energy loss quantum is detectable, with probability $|g_{\text{Qu}}|^2$. Higher EELS orders [44] necessitate a strong coupling $|g_{\text{Qu}}| \sim 1$. In Sec. S.2 of the Supplemental Material [40], strong-coupling EELS is derived as "fieldless PINEM" to touch upon their equivalence. A general feature of the electron-energy distribution is that the average loss is $E_0 - \langle E\rangle = |g_{\text{Qu}}|^2$, in either weak or strong coupling, with and without laser illumination.

For a quantum-optics description of PINEM experiments, one needs to consider a coherent state $|\alpha\rangle$ with an average number of $|\alpha|^2$ photons in the cavity. In this

case, the exact final electron-photon quantum state is characterized by Eq. (1) with the coefficients $c_{n,k}^{\mathrm{PINEM}} = \langle E_k, n|D(\hat{b}g_{\mathrm{Qu}})|E_0,\alpha\rangle$,

$$c_{n,k}^{\mathrm{PINEM}} = e^{(|g_{\mathrm{Qu}}|^2-|\alpha|^2)/2}\frac{\alpha^{(n+k)}g_{\mathrm{Qu}}^k}{\sqrt{n!}}\sum_{\ell=0}^{\infty}\left[\frac{(n+k+\ell)!}{(n+k)!}\right] \times\frac{(-|g_{\mathrm{Qu}}|^2)^\ell}{(k+\ell)!\ell!}. \tag{5}$$

Section S.2 in the Supplemental Material [40] details the algebraic derivation. Figure 2(b) presents the electron-photon spectral probability map for the case of a strong coupling ($g_{\mathrm{Qu}} = 3$) to a cavity populated with nine photons in average, $|\alpha\rangle = |3\rangle$. The entanglement correlates diagonally as for an empty cavity, but also includes rich patterns. Specifically, the electron spectrum depends strongly on the entangled Fock state (see inset for $n = 2$ and $n = 3$). The overall electron spectra is smooth (red bars, top axis), similar to a spatial scattering of atoms off a coherent photon state [45,46]. The electron energy distributes nearly symmetrically around the mean, $-|g_{\mathrm{Qu}}|^2$, with a spectral width of $4|g_{\mathrm{Qu}}\alpha|$. This generalizes PINEM [7,47,48], known for its $4|g|$ bandwidth and for the symmetry around E_0 (special case of $|g_{\mathrm{Qu}}|^2 \to 0$) [8].

To exactly retrieve known PINEM spectra, with probability amplitudes $c_k = J_k(2|g|)$ [8,47], one needs to consider strong optical fields $|\alpha| \gg 1$, weakly coupled to the electron beam $g_{\mathrm{Qu}} \ll 1$. J_k is the Bessel function of the first kind. Conveniently, Eq. (5) reduces to Bessel-function amplitudes when approximating the square brackets within it as

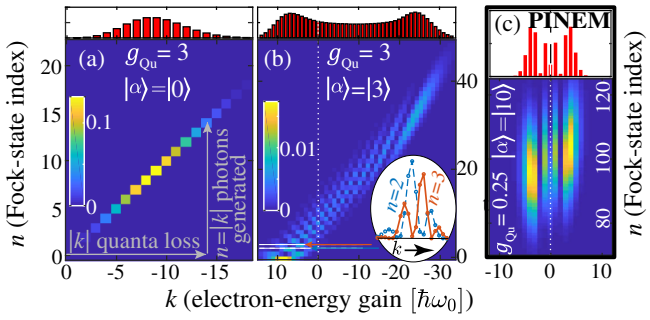

FIG. 2. Electron-photon entanglement patterns. (a) Color map of $|c_{n,k}|^2$, the coincident probabilities of photons with electron-energy gain $k\hbar\omega_0$, after a strong interaction ($g_{\mathrm{Qu}} = 3$) with an empty cavity. (b) Rich entanglement features for an initial coherent state $|\alpha = 3\rangle$, in the cavity. Oscillations in the electron spectra coincident with Fock states (cf. inset for $n = 2$ and $n = 3$) are absent from the integrated electron spectrum (top axis, red bars) since Fock states are orthogonal. (c) The known electron spectrum for PINEM, $|c_k|^2 = |J_k(2|g|)|^2$ (top, red bars), emerges for weak coupling and highly populated cavity ($g_{\mathrm{Qu}} = 0.25$, $|\alpha\rangle = |10\rangle$), with $|g| = |g_{\mathrm{Qu}}\alpha|$. In this limit, the electron and photon states are separable.

$$\frac{(n+k+\ell)!}{(n+k)!} \approx (n+k)^\ell.$$

Thus, one can write $(n+k)^\ell(-|g_{\mathrm{Qu}}|^2)^\ell = (-|g_{\mathrm{Qu}}\sqrt{n+k}|^2)^\ell$. The summation in Eq. (5) then transforms to $(\sqrt{n+k})^{-k}e^{ik\arg g}J_k(2|g|)$, with the definition

$$|g| = |g_{\mathrm{Qu}}\sqrt{n+k}| \approx |g_{\mathrm{Qu}}\alpha|. \tag{6}$$

Neglecting quantum fluctuations added to the light by the interaction $(\sqrt{n+k})^{-k} = (\sqrt{\langle n+k\rangle})^{-k}$ decouples the electron and photon states. Thus, the resulting state

$$|\psi_{\mathrm{PINEM}}\rangle = |\alpha\rangle \otimes J_k(2|g|)|E_k\rangle \tag{7}$$

fully retrieves the known PINEM Bessel amplitudes decoupled from the driving laser field. This decoupling justifies the description of the optically modulated electron wave function, with the natural emergence of the Rabi parameter as $g = g_{\mathrm{Qu}}\alpha$. The reduction of Eq. (5) to Eq. (7) is expanded on in the Supplemental Material, Sec. S.2.2.1 [40]. Figure 2(c) shows the electron-photon spectra for $\alpha = 10$, $g_{\mathrm{Qu}} = 0.25$, that is, a cavity with 100 photons in average, weakly coupled to the electron beam. The electron spectrum is nearly independent of the photon state, yielding the electron spectral oscillations typical for Bessel amplitudes.

The second strong-coupling phenomena exemplified here is the non-Coulombic entanglement of two consecutive electrons in a beam, mediated by long-lived cavity photons. A lifetime of 10 ps allows excitations of the first electron to affect the second, while suppressing Coulombic interactions between them. The passage of the first electron generates a state as in Eq. (4). A second electron with an equal zero-loss energy (marked here $\mathcal{E}_0$ to distinguish it from the first electron) will result in a three-particle state $|\psi_f^{e\text{-}e}\rangle = \sum_{n=0}^{\infty}\sum_{k=-\infty}^{n} c_{n,k}^{e\text{-}e}|E_{-n},\mathcal{E}_k,n-k\rangle$, characterized by two-indices $c_{n,k}^{e\text{-}e} = \langle E_{-n},\mathcal{E}_k,n-k|D(\hat{b}g_{\mathrm{Qu}})|E_{-n},\mathcal{E}_0,n\rangle$. k is the energy quanta gained by the second electron and n is the Fock state index prior to the arrival of the second electron, which is also the final energy state of the first electron $|E_{-n}\rangle$. The final Fock state of the cavity is $|n-k\rangle$. Thus,

$$c_{n,k}^{e\text{-}e} = \frac{g_{\mathrm{Qu}}^{(n+k)}}{n!\sqrt{(n-k)!}}\sum_{\ell=0}^{\infty}(n+\ell)!\frac{(-|g_{\mathrm{Qu}}|^2)^\ell}{(k+\ell)!\ell!}. \tag{8}$$

Detailed derivations are in the Supplemental Material, Sec. S.3 [40]. One can think of such an event as PINEM, pumped by the first electron, as apparent in the similarity of Eqs. (5) and (8). Figure 3 shows the resulting entanglement features for strong couplings of $g_{\mathrm{qu}} = 1$ and $g_{\mathrm{qu}} = 3$. The single particle spectra (right axis, red

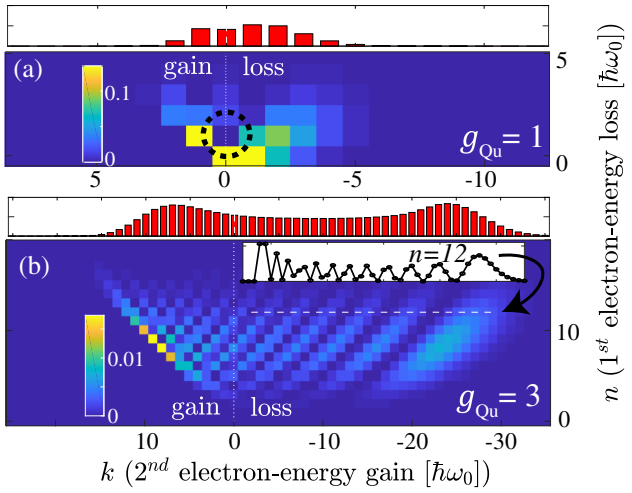

FIG. 3. Electron-electron interaction for two distant electrons in a beam, mediated by long-lived photons. The color map $|c_{n,k}^{e-e}|^2$ is the coincident probability for $n\hbar\omega_0$ energy loss of the first electron and $k\hbar\omega_0$ gain of the second. (a) Strong coupling, $g_{Qu} = 1$, allows for mutually exclusive states (dash circle) of the electron pair, where if the first electron loses one quantum, the second cannot be lossless. (b) Stronger interactions induce rich entanglement features. (Inset) Lineout of the second electron spectra, coincident with $n = 12$.

bars) is smooth, while oscillations appear in coincidence measurements. See the inset of Fig. 3(b) for a spectrum of the second electron, coincident with a 12-quanta-loss state of the first electron. In such an electron-pair experiment, energy gains are unique to the second electron and hence could be used to record coincident spectra without separating the paths of the two electrons.

The last part of this Letter utilizes the above derivations to quantitatively evaluate the coupling constant via PINEM. Specifically, the term $g = g_{Qu}\alpha$ in Eq. (6) links the coupling constant to the classical acceleration of an electron by the mode's field. The field is represented as a coherent state $|\alpha\rangle$, and the acceleration or deceleration is represented by g. For an electron traveling the path $0 < z < L$ near a straight arm of the cavity, the parallel acceleration is given by the light-field component $E_z^{(\omega)}(z, t(z))$, evaluated for time $t(z)$. The superscript ω indicates a frequency dependence. The classically calculated electron-energy gain within the interaction region is $q\int_0^L E_z^{(\omega)}(z, t(z))dz$, where q is the electron charge (transverse recoil is negligible, see Supplemental Material, Sec. S.1.2.2 [40]). g is then the dimensionless ratio between the electron-energy gain and the photon energy [Eq. (3) in Ref. [8]], which with Eq. (6) determines the coupling constant as

$$g_{Qu} = \frac{g}{\alpha} = \frac{1}{\alpha}\frac{q}{2\hbar\omega}\int_0^L E_z^{(\omega)}(z, t(z))dz. \tag{9}$$

Although g_{Qu} is calculated from classical fields, it is a geometrical property of the apparatus for a given electron zero-loss energy, since $|\alpha| = \sqrt{n} \propto E_z$. Intuitively, one can interpret g_{Qu} as the strength of a PINEM effect for one cavity photon. Equation (9) has few important aspects, especially when implemented to a long interaction length, e.g., many microns: (i) The optimal coupling occurs when $E_z^{(\omega)}(z, t(z))$ is constant along the electron trajectory, which is the phase-matching condition. (ii) The field per photon $E_z^{(\omega)}$ scales as $1/\sqrt{L}$ and, for a given waveguide cross section and a given field, the coupling scales as L. Thus, the optimal coupling scales as $\sqrt{L}$. (iii) Conceptually, the ultimate coupling would be for a straight waveguide with periodic boundary conditions and length L. One can realistically reach $1/\sqrt{2}$ of that, when accounting for a backward propagating mode. (iv) The coupling bandwidth is limited by dispersion [see Fig. 1(b)].

A cavity design for a strong coupling requires a small optical-mode volume, matching the velocity of the electron with that of the mode, and a meaningful field component E_z in vacuum. Those can be achieved in WGM cavity, based on a straight single-mode waveguide [see Fig. 1(a)]. The waveguide's width plays multiple roles: it minimizes the mode volume, increases the evanescent tails in vacuum that interact with the electron, increases the field component E_z, and pushes the modal phase velocity towards the speed of the relativistic electrons. The photon lifetime in the cavity has to be substantially longer than the temporal extent of the electron and the time it interacts with the cavity. For example, a quality factor of 500, corresponding to a lifetime of 1500 fs for photons with energies of 1.166 eV, suffices for electron pulses of 200 fs [49], interacting over $L = 100$ μm.

Figure 4 shows the coupling of electron beams to a mode with a photon energy of $\hbar\omega_0 = 1.166$ eV (vacuum

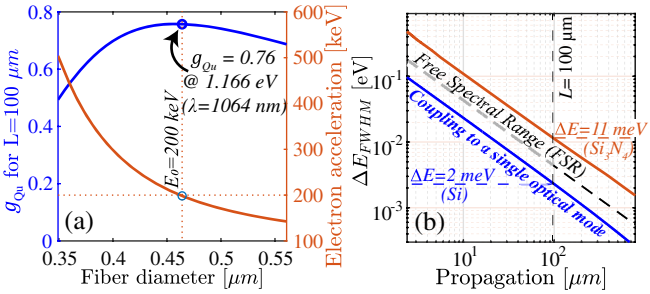

FIG. 4. (a) The coupling constant to a 100-μm-long Si_3N_4 step-index waveguide (left axis, blue) and the phase-matched electron energy (right axis, orange) for 1064 nm photons, as a function of the waveguide diameter. This calculation assumes periodic boundary conditions, thus, a realistic coupling would be smaller by $\sqrt{2}$. (b) The coupling bandwidth (orange) narrows for longer interactions. Increased dispersion (e.g., Si, blue line) can result in a narrower bandwidth than the free spectral range (dash diagonal), which limits the coupling to a single optical mode at most.

wavelength $\lambda = 1064$ nm) in a step index profile [50]. For the selected parameters (100 μm waveguide length with 463 nm diameter, electron zero-loss energy of 200 keV), I find numerically that E_z on the outer surface of a waveguide populated by a coherent state $|\alpha\rangle$ is $0.0177\times|\alpha|$ V/μm. For $|\alpha| = 1$, such a field accelerates an electron by 15 meV/μm. When substituted into Eq. (9), the coupling is $g_{\mathrm{Qu}} = 0.76$ (see more details in Supplemental Material, Sec. S.5.1 [40]). Figure 4(b) presents the spectral width of the interaction, derived from the coherence length [51]. Comparison to the free spectral range for cavities with total circumference of $2L$ (dashed line) indicates the number of modes with which the electron may couple. A Si_3N_4 cavity (orange line) allows for phase matching with four optical modes, while silicon (blue line, for 213 nm diameter) allows for the coupling of a single optical mode, or none.

A racetrack cavity with a 100-μm-long straight arm, mentioned above, and a negligible semicircle circumference can reach a coupling strength of $g_{\mathrm{Qu}} = 0.76/\sqrt{2} = 0.53$, where the $\sqrt{2}$ accounts for the noninteracting cavity arm. The field evanescence length in vacuum is 120 nm. Thus, an electron beam with a semiconvergence angle of 0.15 mrad and a waist of 10 nm would experience a uniform light field. These are achievable parameters in contemporary electron microscopes. With this design scheme, unprecedented strong-coupling and long-lived entanglement effects may be reached in the not-distant future.

To conclude, this Letter proposes a path towards a strong-coupling regime between electrons and cavity photons based on narrow-band phase matching and investigates phenomena that this regime may enable. The analytical model addresses EELS and PINEM on an equal footing alongside strong-coupling phenomena. The coupling g_{Qu}, which can be understood as the PINEM Rabi parameter g per one driving photon, may be retrieved experimentally using PINEM, via Eq. (9), or using EELS via the energy loss probability $|g_{\mathrm{Qu}}|^2$, per optical mode. Additionally, strong coupling to a cavity can entwine the quantum state of two consecutive electrons, entangling their final energies. These phenomena, and the concrete design approach brought here, set a road map for experiments on free electrons strongly coupled with photons. In the future, the ability to imprint quantum-optical states on relativistic electron beams may enable the use of electrons as information carriers. The fundamental differences between light and electrons may open new horizons. One example is the use of the high efficiency of electron detection to herald single- or multiple-photon sources. Another is long-distance communication in outer space, where matter beams exhibit superior divergence properties and allow for manipulation with electric and magnetic fields.

This project has received funding from the European Union's Horizon 2020 research and innovation programme under the Marie Skłodowska-Curie Grant Agreement No. 752533. I gratefully acknowledge Sergey V. Yalunin, Hugo Lourenço-Martins, Armin Feist, and Claus Ropers for illuminating discussions and support.

*ofer.kfir@phys.uni-goettingen.de

[1] A. Einstein, B. Podolsky, and N. Rosen, Can quantum-mechanical description of physical reality be considered complete?, Phys. Rev. **47**, 777 (1935).
[2] G. Weihs, T. Jennewein, C. Simon, H. Weinfurter, and A. Zeilinger, Violation of Bell's Inequality under Strict Einstein Locality Conditions, Phys. Rev. Lett. **81**, 5039 (1998).
[3] A. Aspect, Bell's inequality test: More ideal than ever, Nature (London) **398**, 189 (1999).
[4] M. A. Nielsen and I. L. Chuang, *Quantum Computation and Quantum Information*, 10th ed. (Cambridge University Press, Cambridge, England, 2010).
[5] S. Wengerowsky, S. K. Joshi, F. Steinlechner, J. R. Zichi, S. M. Dobrovolskiy, R. van der Molen, J. W. N. Los, V. Zwiller, M. A. M. Versteegh, A. Mura, D. Calonico, M. Inguscio, H. Hübel, L. Bo, T. Scheidl, A. Zeilinger, A. Xuereb, and R. Ursin, Entanglement distribution over a 96-km-long submarine optical fiber, Proc. Natl. Acad. Sci. U.S.A. **116**, 6684 (2019).
[6] J. Yin *et al.*, Satellite-to-Ground Entanglement-Based Quantum Key Distribution, Phys. Rev. Lett. **119**, 200501 (2017).
[7] B. Barwick, D. J. Flannigan, and A. H. Zewail, Photon-induced near-field electron microscopy, Nature (London) **462**, 902 (2009).
[8] A. Feist, K. E. Echternkamp, J. Schauss, S. V. Yalunin, S. Schäfer, and C. Ropers, Quantum coherent optical phase modulation in an ultrafast transmission electron microscope, Nature (London) **521**, 200 (2015).
[9] C. Kealhofer, W. Schneider, D. Ehberger, A. Ryabov, F. Krausz, and P. Baum, All-optical control and metrology of electron pulses, Science **352**, 429 (2016).
[10] K. E. Echternkamp, A. Feist, S. Schäfer, and C. Ropers, Ramsey-type phase control of free-electron beams, Nat. Phys. **12**, 1000 (2016).
[11] G. M. Vanacore, I. Madan, G. Berruto, K. Wang, E. Pomarico, R. J. Lamb, D. McGrouther, I. Kaminer, B. Barwick, F. J. G. de Abajo, and F. Carbone, Attosecond coherent control of free-electron wave functions using semi-infinite light fields, Nat. Commun. **9**, 2694 (2018).
[12] K. E. Priebe, C. Rathje, S. V. Yalunin, T. Hohage, A. Feist, S. Schäfer, and C. Ropers, Attosecond electron pulse trains and quantum state reconstruction in ultrafast transmission electron microscopy, Nat. Photonics **11**, 793 (2017).
[13] Y. Morimoto and P. Baum, Diffraction and microscopy with attosecond electron pulse trains, Nat. Phys. **14**, 252 (2018).
[14] M. Kozák, N. Schönenberger, and P. Hommelhoff, Ponderomotive Generation and Detection of Attosecond Free-Electron Pulse Trains, Phys. Rev. Lett. **120**, 103203 (2018).
[15] F. J. García de Abajo and M. Kociak, Electron energy-gain spectroscopy, New J. Phys. **10**, 073035 (2008).
[16] P. Das, J. D. Blazit, M. Tencé, L. F. Zagonel, Y. Auad, Y. H. Lee, X. Y. Ling, A. Losquin, C. Colliex, O. Stéphan, F. J. García de Abajo, and M. Kociak, Stimulated electron energy

loss and gain in an electron microscope without a pulsed electron gun, Ultramicroscopy **203**, 44 (2019).
[17] D. L. Freimund, K. Aflatooni, and H. Batelaan, Observation of the Kapitza–Dirac effect, Nature (London) **413**, 142 (2001).
[18] O. Schwartz, J. J. Axelrod, S. L. Campbell, C. Turnbaugh, R. M. Glaeser, and H. Müller, Laser control of the electron wave function in transmission electron microscopy, arXiv: 1812.04596.
[19] A. Campos, N. Troc, E. Cottancin, M. Pellarin, H.-C. Weissker, J. Lermé, M. Kociak, and M. Hillenkamp, Plasmonic quantum size effects in silver nanoparticles are dominated by interfaces and local environments, Nat. Phys. **15**, 275 (2019).
[20] F. J. García de Abajo, Optical excitations in electron microscopy, Rev. Mod. Phys. **82**, 209 (2010).
[21] N. Talebi, Interaction of electron beams with optical nanostructures and metamaterials: from coherent photon sources towards shaping the wave function, J. Opt. **19**, 103001 (2017).
[22] E. J. R. Vesseur, F. J. G. de Abajo, and A. Polman, Broadband Purcell enhancement in plasmonic ring cavities, Phys. Rev. B **82**, 165419 (2010).
[23] G. Unger, A. Trügler, and U. Hohenester, Novel Modal Approximation Scheme for Plasmonic Transmission Problems, Phys. Rev. Lett. **121**, 246802 (2018).
[24] M. J. Lagos, A. Trügler, U. Hohenester, and P. E. Batson, Mapping vibrational surface and bulk modes in a single nanocube, Nature (London) **543**, 529 (2017).
[25] S. V. Yalunin, B. Schröder, and C. Ropers, Theory of electron energy loss near plasmonic wires, nanorods, and cones, Phys. Rev. B **93**, 115408 (2016).
[26] A. Hörl, A. Trügler, and U. Hohenester, Tomography of Particle Plasmon Fields from Electron Energy Loss Spectroscopy, Phys. Rev. Lett. **111**, 076801 (2013).
[27] G. Haberfehlner, F.-P. Schmidt, G. Schaffernak, A. Hörl, A. Trügler, A. Hohenau, F. Hofer, J. R. Krenn, U. Hohenester, and G. Kothleitner, 3D imaging of gap plasmons in vertically coupled nanoparticles by EELS tomography, Nano Lett. **17**, 6773 (2017).
[28] Y. Yang, A. Massuda, C. Roques-Carmes, S. E. Kooi, T. Christensen, S. G. Johnson, J. D. Joannopoulos, O. D. Miller, I. Kaminer, and M. Soljačić, Maximal spontaneous photon emission and energy loss from free electrons, Nat. Phys. **14**, 894 (2018).
[29] I. Kaminer, S. E. Kooi, R. Shiloh, B. Zhen, Y. Shen, J. J. López, R. Remez, S. A. Skirlo, Y. Yang, J. D. Joannopoulos, A. Arie, and M. Soljačić, Spectrally and Spatially Resolved Smith-Purcell Radiation in Plasmonic Crystals with Short-Range Disorder, Phys. Rev. X **7**, 011003 (2017).
[30] N. Talebi, A directional, ultrafast and integrated few-photon source utilizing the interaction of electron beams and plasmonic nanoantennas, New J. Phys. **16**, 053021 (2014).
[31] S. Guo, N. Talebi, A. Campos, M. Kociak, and P. A. van Aken, Radiation of Dynamic Toroidal Moments, ACS Photonics **6**, 467 (2019).
[32] P. Das, H. Lourenço-Martins, L. H. G. Tizei, R. Weil, and M. Kociak, Nanocross: A highly tunable plasmonic system, J. Phys. Chem. C **121**, 16521 (2017).
[33] H. Lourenço-Martins, P. Das, L. H. G. Tizei, R. Weil, and M. Kociak, Self-hybridization within non-Hermitian localized plasmonic systems, Nat. Phys. **14**, 360 (2018).
[34] P. Schattschneider and S. Löffler, Entanglement and decoherence in electron microscopy, Ultramicroscopy **190**, 39 (2018).
[35] D.-L. Hornauer, Light scattering experiments on silver films of different roughness using surface plasmon excitation, Opt. Commun. **16**, 76 (1976).
[36] T. Inagaki, K. Kagami, and E. T. Arakawa, Photoacoustic observation of nonradiative decay of surface plasmons in silver, Phys. Rev. B **24**, 3644 (1981).
[37] A. Gover and Y. Pan, Dimension-dependent stimulated radiative interaction of a single electron quantum wavepacket, Phys. Lett. A **382**, 1550 (2018).
[38] Y. Pan, B. Zhang, and A. Gover, Anomalous Photon-Induced Near-Field Electron Microscopy, Phys. Rev. Lett. **122**, 183204 (2019).
[39] M. O. Scully and M. S. Zubairy, *Quantum Optics* (Cambridge University Press, Cambridge, England, 1997).
[40] See Supplemental Material at http://link.aps.org/supplemental/10.1103/PhysRevLett.123.103602 for detailed and elaborated derivations, which includes Refs. [41,42].
[41] L. Mandel and E. Wolf, *Optical Coherence and Quantum Optics* (Cambridge University Press, Cambridge, England, 1995).
[42] C. Yeh, Guided-wave modes in cylindrical optical fibers, IEEE Trans. Ed. **E-30**, 43 (1987).
[43] R. J. Glauber, Coherent and incoherent states of the radiation field, Phys. Rev. **131**, 2766 (1963).
[44] F. J. García de Abajo, Multiple excitation of confined graphene plasmons by single free electrons, ACS Nano **7**, 11409 (2013).
[45] V. M. Akulin, F. L. Kien, and W. P. Schleich, Deflection of atoms by a quantum field, Phys. Rev. A **44**, R1462 (1991).
[46] A. M. Herkommer, V. M. Akulin, and W. P. Schleich, Quantum Demolition Measurement of Photon Statistics by Atomic Beam Deflection, Phys. Rev. Lett. **69**, 3298 (1992).
[47] S. T. Park, M. Lin, and A. H. Zewail, Photon-induced near-field electron microscopy (PINEM): Theoretical and experimental, New J. Phys. **12**, 123028 (2010).
[48] S. T. Park and A. H. Zewail, Relativistic effects in photon-induced near field electron microscopy, J. Phys. Chem. A **116**, 11128 (2012).
[49] A. Feist, N. Bach, N. Rubiano da Silva, T. Danz, M. Möller, K. E. Priebe, T. Domröse, J. G. Gatzmann, S. Rost, J. Schauss, S. Strauch, R. Bormann, M. Sivis, S. Schäfer, and C. Ropers, Ultrafast transmission electron microscopy using a laser-driven field emitter: Femtosecond resolution with a high coherence electron beam, Ultramicroscopy **176**, 63 (2017).
[50] C.-L. Chen, *Foundations for Guided-Wave Optics* (John Wiley & Sons, New York, 2006).
[51] R. W. Boyd, *Nonlinear Optics*, 2nd ed. (Academic Press, New York, 2003).